Available online at www.sciencedirect.com
SCIENCE DIRECT®
Composites Science and Technology 65 (2005) 2550–2562
COMPOSITES SCIENCE AND TECHNOLOGY
www.elsevier.com/locate/compscitech

Strengths of C/C composites under tensile, shear, and compressive loading: Role of interfacial shear strength

Hiroshi Hatta [a,*], Ken Goto [a], Takuya Aoki [b]

[a] Institute of Space and Astronautical Science, Japan Aerospace Exploration Agency, 3-1-1 Yoshijnodai, Sagamihara, Kanagawa 229-8510, Japan
[b] Institute of Space Technology and Aeronautics, Japan Aerospace Exploration Agency, 6-13-1 Ohsawa, Mitaka, Tokyo 181-0015, Japan

Received 1 April 2005; received in revised form 8 July 2005; accepted 12 July 2005
Available online 24 August 2005

Abstract

Various strengths of carbon–carbon composites (C/Cs) are comprehensively reviewed. The topics reviewed include tensile, shear, compressive, and fatigue strength as well as fiber/matrix interfacial strength of C/Cs. When data are available, high temperature properties, including creep behavior, are presented. Since C/Cs have extremely low fiber/matrix interfacial strength τ_d, the interfacial fracture plays important roles in all of the fracture processes dealt in this review. The low τ_d was found to divide tensile fracture units into small bundles, to seriously degrade both shear and compressive strength, and to improve fatigue performance. In spite of the importance of the interfacial strength of C/Cs, techniques for its evaluation and analysis are still in a primitive stage.
© 2005 Elsevier Ltd. All rights reserved.

Keywords: A. Carbon fibers; B. Interfacial strength; Strength; Stress/strain curves

1. Introduction

Carbon fiber-reinforced carbon matrix composites (C/Cs) exhibit superior thermo-mechanical properties even at elevated temperatures above 2000 K. In light of this advantage, C/Cs are expected to be applicable for use in high-temperature structures [1–4]. However, the mechanical behavior of C/Cs has not been fully elucidated to the extent that their mechanical properties can be tailored to certain purposes as in the cases with fiber-reinforced plastics and ceramics. Thus, C/C structures have been designed on a trial-and-error basis, and therefore lack sufficient reliability for use in primary load-bearing structures. As a result, the applications of C/Cs have been restricted to structures in which high strength is not required, but rather in which only high-temperature capabilities are necessary. Recently, the present authors and their colleagues have expended a significant amount of effort toward the clarification of the mechanical behavior of C/Cs especially from the viewpoint of fracture mechanisms [5–10]; thus far, most of fracture processes of C/Cs have been found to profoundly affected by their fiber/matrix interfacial properties. The present review deals with such recent progress regarding the strengths of C/Cs, including studies of their tensile, shear, compressive, and fatigue strength as well as fiber/matrix interfacial strength. Based on recent findings, special attention is paid to the relationship between these fracture mechanisms and the roles played by fiber/matrix interfacial strength.

2. Fiber/matrix interface of C/Cs

2.1. Interfacial shear strength at room temperature

Several attempts have been made to measure the fiber/matrix interfacial shear strength of C/Cs using

* Corresponding author. Tel +81 42 759 8293; fax +81 42 759 8461.
E-mail addresses: hatta@isas.jaxa.jp, hatta@pub.isas.ac.jp (H. Hatta).

0266-3538/$ - see front matter © 2005 Elsevier Ltd. All rights reserved.
doi:10.1016/j.compscitech.2005.07.012

methods often adopted for other composites, i.e., polymer matrix and ceramic matrix composites [11–17], including fiber push-in, push-out, and pull-out tests [18–22]. However, to date, the interfacial shear strength of C/Cs has been successfully determined only by fiber push-out tests [9,21,22]. The difficulties associated with the determination of the interfacial strength of C/Cs are twofold. First, the carbon fiber is prone to compressive failure upon compressive axial loading. This tendency is especially noticeable in the case of pitch-derived fibers. Accordingly, a specimen must be prepared such that interfacial debonding readily occurs at a sufficiently low load. This means that the specimen should be extremely thin and less than approximately 100 μm. However, in such a case, the fiber/matrix interface is often damaged during specimen preparation. The second difficulty in this context is the thickness of the carbon fibers, which are around 5–10 μm in diameter. Hence, the application of load precisely at the center of fiber cross-sections and confirmation of damage at such an interface remain rather difficult [21]. Thus, the utilization of the single fiber push-out test was limited to polyacrylonitrile (PAN)-based carbon fibers, and to specimens with weak interfaces.

In order to avoid such difficulties, we attempted a fiber bundle push-out test. The procedure of this test is illustrated in Fig. 1. In this test, an indenter with 50 μm in diameter was successfully employed [9,23]. Thus, the diameter of pushed-out bundle is large and the thickness of specimen can be set about 100–300 μm. Observation of pushed-out bundles ensured that fiber/matrix interfacial fracture dominated fracture surface. This result guaranteed reliability of this test method. However, the single and bundle push-out tests resulted in different interfacial strengths [21]. Accordingly, the present methods are useful in comparative purpose, but insufficient for measurements of quantitative physical values.

Typical results obtained by the fiber bundle push-out tests are shown in Figs. 2 [9] and 3 [24,25] for C/Cs reinforced with PAN-based fiber IM-600 and pitch-based fibers K321 and K633, respectively. In Fig. 2, 2D-RC-2573K and 2D-HIP-2573K represent IM-600-C/Cs with cross-ply lamination (2D) densified by the resin char method (RC) or the hot isostatic pressing method (HIP) and heat-treated at 2573 K. The fiber volume fraction (V_f) in the precursor (carbon fiber-reinforced phenolic resin) of these C/Cs was 60%. As this figure shows, the interfacial sliding stress τ_s and the debonding stress τ_d were enhanced with increase in density ρ, and the ultimate tensile fracture strain ε_b was degraded with

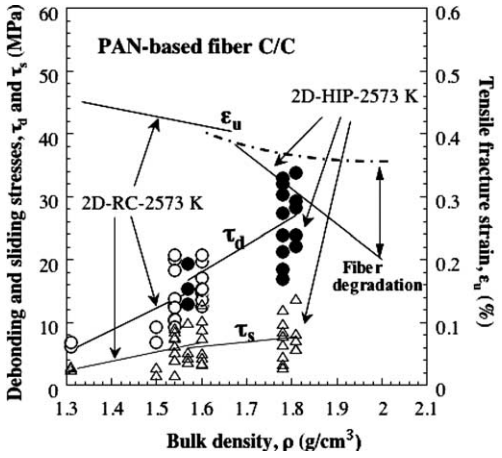

Fig. 2. Tensile fracture strain, ε_u, interfacial debonding stress, τ_d, and interfacial sliding stress, τ_s, of a cross-ply-laminated C/C reinforced with PAN-based fiber IM600 as a function of bulk density, ρs densified by the repeating resin char method (RC) and the hot isostatic pressuring method (HIP) [9].

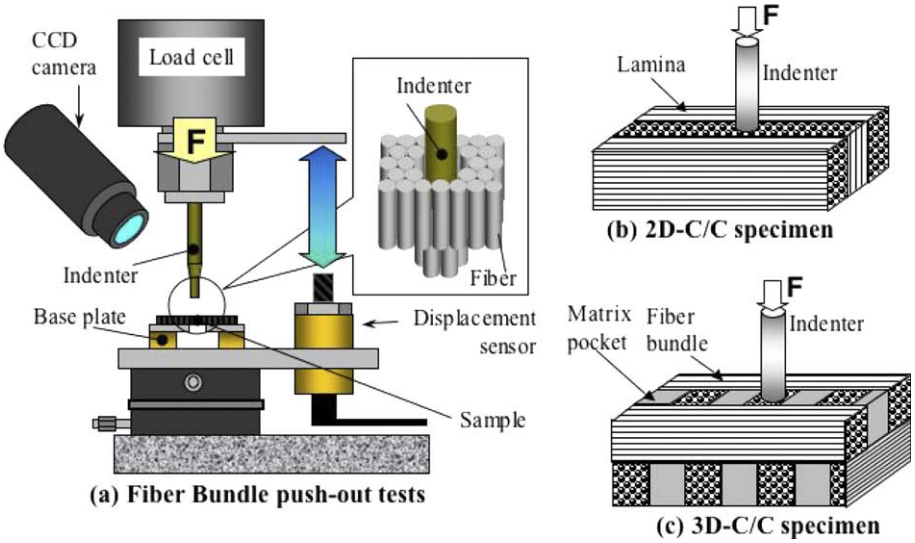

Fig. 1. Schematic drawings of the fiber bundle push-out test. Test fixture (a), specimen arrangement for 2D-C/C (b) and 3D-C/C (c).

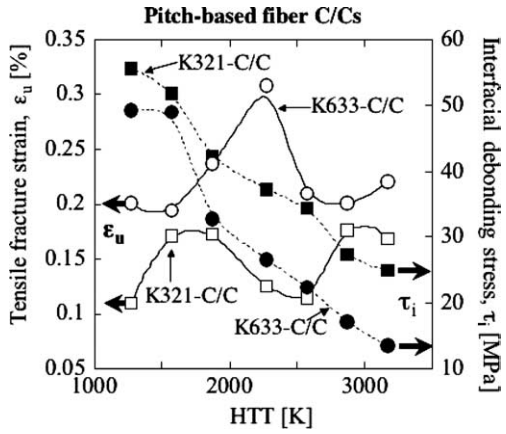

Fig. 3. Tensile fracture strain, ε_u, and interfacial debonding stress of cross-ply-laminated C/Cs reinforced with pitch-based fiber K321 and K633 as a function of heat treatment temperature, HTT, densified by 5 cycles of hot isostatic pressuring (HIP) [23,24].

ρ. By the densification, interfacial debonding is gradually eliminated, as it is clear from a comparison of the photos in Figs. 4(a) and (b). This reduction of debonded interfaces with increasing ρ is the most influential factor for enhancing interfacial strength of this material.

In Fig. 3, the τ_ds of K321-C/C and K633-C/C are shown as a function of the heat treatment temperature (HTT). The τ_ds of these C/Cs clearly decrease with increases in HTT. The decrease in the τ_ds was partly due to the extension of fiber/matrix-interfacial debonding with increasing HTT, as shown in Fig. 4(c) and (d). This development of debonding was facilitated primarily by the development of graphitization in the matrix [25]. The other source of the reduction in τ_d in this case was found to be a reduction in the bonding strength of truly bonded interfaces due to graphitization, by

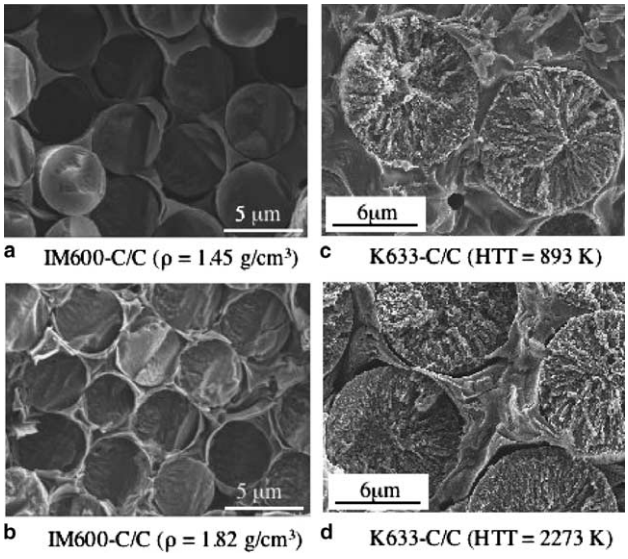

Fig. 4. Cross-sections of IM600 C/Cs (a) and (b) with different densities, ρs, and K633-C/Cs (c) and (d) heat-treated at different temperatures [9,25].

which the crystalline units increased in size and the (002) surfaces were aligned in a more parallel manner with the interfaces [26]. The lowest values of the τ_ds shown in Figs. 2 and 3 are nearly the same as those of CFCCs with weak interface and high tensile elongation.

2.2. Interfacial shear strength at elevated temperatures

In order to examine the interfacial debonding stress at elevated temperatures, a specially arranged fiber bundle push-out test was conducted using the specimen shown in Fig. 5 [22]. Note that in this figure, the specimen was assumed to be an orthogonally reinforced (3D)-C/C. The push-out test specimen had a rectangular cross-section with a circumferential notch around the loading fiber bundle located at the center of the cross-section. The notch was introduced perpendicular to the loading (z-) bundle up to a depth of 0.05–0.15 mm in the loading bundle; the notch was created by a diamond wheel saw with a thickness of 0.8 mm. A compressive load was applied directly at the top end of the specimen; the z-bundle was extruded in a hole machined at the bottom of the specimen. This type of specimen did not require a supporting test fixture. Thus, high temperature testing can be performed without considering the effect of thermal mismatch stress between the specimen and the test fixture. The fiber bundle interfacial debonding stress τ_d was determined based on the maximum load divided by the debonded area.

Fig. 6 [22] summarizes the temperature dependence of the fiber bundle interfacial debonding stress τ_d of 3D-C/C as a function of the test temperature, T. As it is clearly seen in this figure, τ_d monotonically increases with increasing T. Observations of cross-sections of as-tested specimens revealed that push-out fractures occurred primarily within the carbon matrices that created bonds between adjacent fiber bundles. The matrix in C/Cs

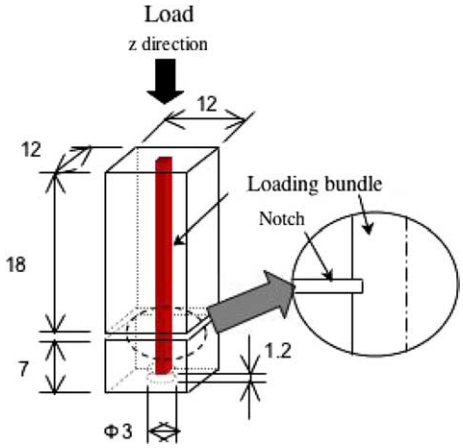

Fig. 5. Shape and dimensions of fiber bundle push-out specimen for determination of interfacial shear strength at elevated temperatures. The material of this test is assumed to be three-dimensionally reinforced C/Cs [22].

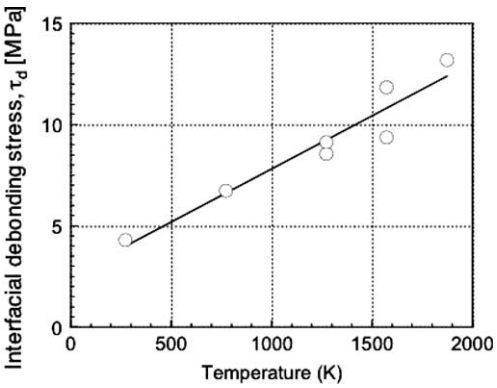

Fig. 6. Temperature dependence of the fiber/matrix interfacial debonding stress, τ_d, of the 3D-C/C [22], reinforced with PAN-based carbon fiber, T-300, heat-treated at 2773 K, and a total fiber volume fraction of 48% (16% in each direction).

shrinks to a great extent during the processing, at the carbonization stage, due to the conversion of resin into carbon, and the cooling stage from the heat treatment temperature to room temperature by reversed thermal expansion. Hence, significant tensile thermal stresses accumulate in the matrix of C/Cs [27] in the directions parallel to and perpendicular to the fiber/matrix interface. These tensile stresses reduce the τ_d. Thus, the dominant mechanism leading to increases in τ_d at elevated temperatures is thought to be the relief of thermal stresses in carbon matrices at the fiber bundle interfaces.

3. Tensile strength

3.1. Parameters determinative of tensile fracture

The tensile strength of C/Cs is typically much weaker than that expected from a rule of mixtures [8,23]. In order to identify the mechanisms producing such low strength, the effects of various potential factors including the heat treatment temperature [28,29], the fiber/matrix interfacial strength [30,31], and defects in the C/Cs [32–35] have been investigated. Continuous fiber-reinforced ceramic matrix composites (CFCCs) are also known to elongate to a much lesser degree than do reinforcing fibers [36,37]. Statistical models have been proposed [38–41] to account for the tensile strength of CFCCs, in which the fiber/matrix interfacial sliding stress τ_s has been assumed to support a portion of the tensile load. Recently, a model proposed by Curtin et al. [38,39] has attracted attention for its successful prediction of the tensile fracture stress of CFCCs, which is higher than the strength of dry fiber bundle and slightly enhanced with increase in τ_s. C/Cs usually exhibit the opposite tendency [9,23,26,30,31]; the tensile strength of C/Cs was lower than that of the dry bundle and was found to improve with decrease in interfacial bonding, τ_d. Thus, a new model is required in order to simulate the tensile fracture of C/Cs.

Hatta et al. recently examined the effects of density on the tensile strength of various C/Cs, and they reconfirmed that the tensile strength of the C/Cs decreased with the enhancement of matrix/fiber interfacial strength, τ_d, [9] as shown in Fig. 2. The 2D-HIP-2573K samples shown in this figure degraded more rapidly than did 2D-RC-2573K specimens. This was found to be due to fiber degradation, which occurred only in the case of 2D-HIP-2573K samples by simultaneous and repeated applications of a high pressure and high temperature, HIP treatment [9]. In this figure, the tensile fracture strain was diminished with density, ρ. This result is superficially not in agreement with findings reported in other studies of the densification effect; the tensile strength of C/Cs has been often reported to increase with ρ when C/C density is rather low [42]. However, if one considers the data of 2D-RC-2573K in Fig. 2, in which the tensile fracture stress is plotted instead of strain, then revised data demonstrates that the fracture stress increases with ρ [9]. This behavior can be explained in terms of Young's modulus E; much lower Young's moduli than the predictions by a rule of mixtures are obtained when low density C/Cs are used in ordinary tensile test set up. Since low density C/Cs have extremely low interfacial strengths. In such circumstances, the load from the tensile test fixture of a tensile loading machine to the surfaces of a specimen was not transferred to the core (center region) of specimen. Thus, low density C/C tends to be loaded only in near surface regions [9]. This non-uniform stress across a cross-section of a tensile specimen led to low Young's moduli and low strength, though maintaining high tensile fracture strain near surface region.

Fig. 3 shows the tensile fracture strain ε_us and interfacial shear strength τ_ds of pitch-fiber reinforced C/Cs as a function of heat treatment temperature, HTT [24]. In this figure, the relationship between the ε_us and τ_ds appears rather complicated; although the τ_ds monotonically decrease with HTT, the ε_us show more complex behaviors. This behavior of the ε_us was explained in terms of fiber degradation [24]. The strengths of K633 and K321 fibers were found to suddenly decrease from 2300 and 1800 K (speculated to be HTTs of the fibers), respectively. Thus, Figs. 2 and 3 suggest that the tensile fracture strains of C/Cs can be determined on the basis of fiber strength and interfacial strength, provided that statistical distributions of both are included [26].

The tensile fracture surfaces of K633-C/Cs heat-treated at various temperatures are shown in Fig. 7. As this figure shows, the tensile fracture of C/Cs occurred by intermittent fractures by fiber bundle units; the thicknesses of the fractured fiber bundles consistently decreased with decrease in τ_d. This tendency was also observed in the cases of the K321-C/Cs and IM600-C/

Cs (the 2D-HIP-2573K and 2D-RC-2573K in Fig. 2). In spite of low interfacial strength, the brittle (bundle unit) tensile-fractures were derived for C/Cs. It is due to low toughness of carbon fibers [26]. When a matrix crack arrives at fiber/matrix interface, the direction of crack extension can be evaluated, for example, by the following equation given by Kendall [43]:

$$\frac{G_{ic}}{G_{fc}} \leqslant \left(\frac{h_m E_m + h_f E_f}{h_f E_f}\right)\left[\frac{1}{4\pi(1-v^2)}\right], \quad (1)$$

where G_c, h, and v are critical energy release rate, thickness (two-dimensional model), and Poisson ratio. The subscripts f and m represent fiber and matrix. When this inequality is satisfied, crack at the interface reflects to the interface, respectively. Representative G_{fc}s of PAN-based carbon fiber and SiC fiber are 7.5 and 54.5 J/m^2 [44,45], respectively. Substitution of typical values of C/C and SiC/SiC into Eq. (1) revealed that a matrix crack tends to penetrate into fiber for C/Cs, but to deflect to the interface for example SiC/SiC [26].

Above result suggests the following sequence as a possible tensile fracture process of C/Cs [26].

(1) A crack initiated from single fiber fracture penetrates through fibers until the crack tip meets interfaces possessing an extremely low τ_d. At such location, the crack front is deflected toward interface. Thus, the fracture bundle is determined by the probability of encountering an extremely weak interface. As shown in Fig. 2, interfacial debonding stress was scattered very widely. This result indicates that when the average τ_d is high, then the fracture bundles are thick.
(2) The type of bundle-unit-fractures described above intermittently continues to proceed.
(3) The load, which was sustained by broken bundles, is nearly uniformly transferred to surviving fibers, because the τ_d is extremely low in the C/Cs.
(4) When the remaining fibers cannot sustain the load, then the ultimate fracture occurs. Thus, the ultimate fracture occurs earlier when fracture bundle is thicker, because the transferred load per fractured bundle is higher.

Thus, the tensile fracture stress of C/Cs can be predicted if we can determine the fracture fiber bundle by a simulation of fracture process of each fiber bundle using, for example, a Monte Carlo method. For a specially arranged mini-bundle C/C, fracture bundle could be easily determined and a Monte Carlo simulation resulted in excellent agreement with experimentally obtained C/C strength [46].

3.2. Tensile properties at high temperatures

Only a small number of reports have been published concerning high-temperature behavior [3,4,8,47–49], and the results have been contradictory, even with respect to the temperature dependence of tensile and flexural strength. Fig. 8 shows the typical tensile stress–strain, σ–ε curves of a cross-ply laminate C/C (CP) loaded in the 0° (fiber axis) direction at room temperature and 2273 K, and obtained at a crosshead speed of 0.1 or 5.0 mm/min [8]. As shown in this figure, the σ–ε curve of the C/C at room temperature was linear up to the point of total fracture, and the same line was traced during the repetition of loading–unloading. In contrast, a nonlinear deformation and permanent strain were observed at 2273 K at a test speed of 0.1 mm/min. However, the σ–ε curve at a test speed of 5.0 mm/min resulted in a nearly straight line up to the total fracture,

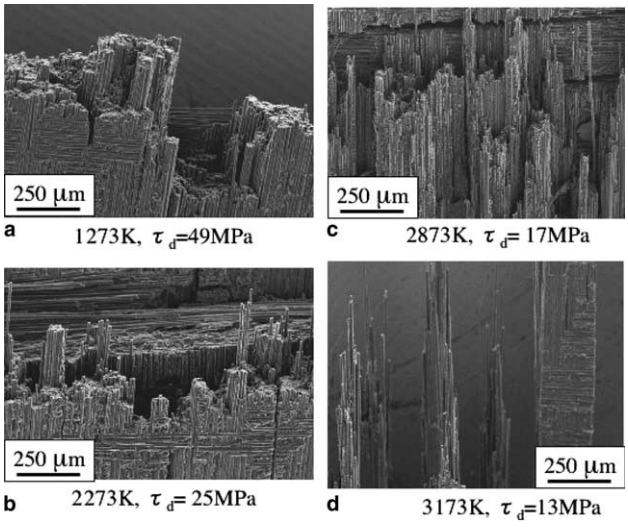

Fig. 7. Comparison of tensile fracture surfaces of K633 C/Cs heat-treated at the designated temperatures with different interfacial shear debonding stresses, τ_d [26].

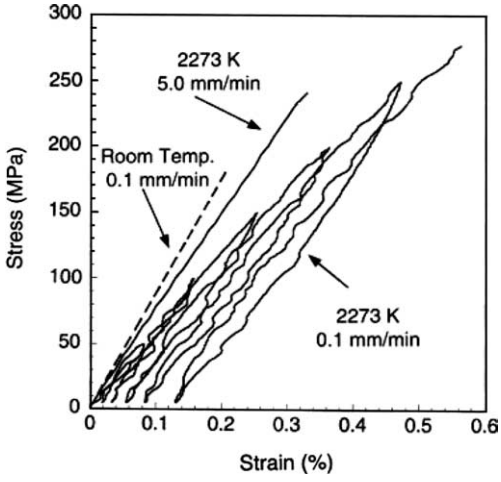

Fig. 8. Stress–strain curves of a cross-ply-laminated C/C at room temperature and at 2273 K, with different crosshead speeds of 0.1 and 5.0 mm/min [8].

with a slight decrease in Young's modulus, compared with the results obtained at room temperature shown as a broken line in Fig. 8. These findings indicate that, at elevated temperatures, the σ–ε curves of C/Cs are similar to those at room temperature, and apparent nonlinear behavior appears due to a strain rate-dependent factor, i.e., creep deformation.

The reported results regarding the temperature dependence of tensile and flexural strength have been contradictory; while some researchers have reported a weak dependence on temperature [3,4,47], others have shown a significant enhancement of strength [4,8,48,49]. To elucidate the mechanisms governing the enhancement of the strength of C/Cs at high temperatures, tensile tests of a 2D-laminate C/C parallel to the fiber axis were conducted at various temperatures up to 2773 K [8]. The tensile strength of the C/C was monotonically enhanced with increase in temperature, as shown in Fig. 9. This enhancement became rapid from 1773 K. One of the mechanisms responsible for this enhancement in strength was the de-gassing of absorbed water [8], which exerted a dominant influence on the enhancement in tensile strength observed at temperatures up to 1773 K [8]. The strength degradation by absorbed water has already been observed under shear and bending loads [49–52]. It was speculated that absorbed water weakens chemical carbon bonding. Thus, at elevated temperatures under vacuum, absorbed gas evaporated and original higher strength was recovered. The second mechanism was the enhancement of the strengths of the fibers and matrix due to stretching graphitization that took place during creep deformation [8]. This phenomenon was especially notable at temperatures exceeding 1773 K, and it produced much greater levels of enhancement than did de-gassing.

3.3. Creep behavior

Creep deformation in the C/C has been reported at temperatures exceeding 1773 K [8,53,54], as shown in Fig. 10 in the case of a 2D laminate C/C reinforced with M40 carbon fiber (M40-C/C). In this experiment, the tensile creep behavior was observed until a creep strain of 10%, but no creep rupture was observed. More rapid creep behavior was observed for a C/C reinforced with high-strength type carbon fiber T300, Toray [8,54]. Generally, creep rates have been compared in terms of steady-state creep, where the creep rate is constant. As regards steady-state creep rate $d\varepsilon/dt$, the Dorn equation [55], given by Eq. (2), has frequently been adopted. The Dorn equation is characterized by the stress exponent, n, and the activation energy, Q, as follows:

$$d\varepsilon/dt = A\sigma^n \exp(-Q/RT), \tag{2}$$

where A is a constant, R is the gas constant, and T is the test temperature. From Fig. 10, n and Q were determined to be 2.0 and 1100 kJ/mol, respectively, and those of a C/C reinforced with T300 were 6.0 and 730 kJ/mol, respectively; here, the Q value of these two C/Cs appears similar, but n is different. A similar Q value has been reported for other C/Cs [53] and glassy carbons [56], i.e., from 1000 to 1200 kJ/mol. As regards the value of n in the case of carbon materials, 6.0 [54] and 8.0 [53,56] have been reported. These values indicate that different fiber results in different value of n, but in similar Q values. However, the underlying mechanisms for these results have not been elucidated.

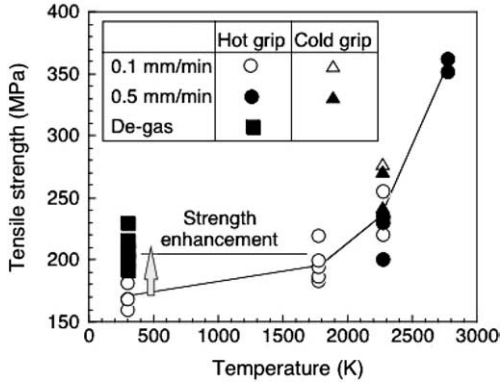

Fig. 9. Temperature dependence of tensile strength in a cross-ply-laminated C/C (reinforced with high modulus carbon-fiber M40 Toray) obtained under a vacuum at temperatures of up to 2273 K and an Ar atmosphere at temperatures above 2273 K. The difference between C/C strengths with and without de-gassing treatment represents the effect of absorbed water. The de-gassing treatment was carried out at 1473 K under a vacuum. The strength improvement at temperatures of up to 1773 K was due to the evaporation of absorbed gas, whereas the improvement at temperatures above 1773 K was caused by creep deformation [8].

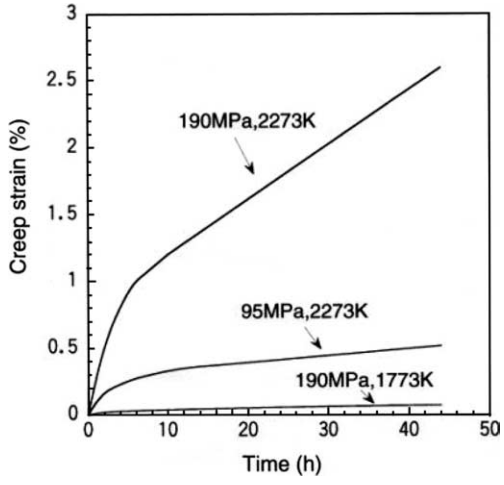

Fig. 10. Creep curves of cross-ply-laminated C/Cs reinforced with high-modulus fiber M40 [8].

4. Shear strength

4.1. Stress–strain curve

Although C/Cs exhibit high strength and a linear σ–ε curve in terms of tension parallel to a fiber axis (Fig. 8), a significant non-linearity in the stress–strain curve followed by extremely low strength appears in cases involving shear loading [57,58]. This characteristic has been reported to be most salient feature of C/Cs in comparison with CFCCs [37]. In particular, three-dimensionally reinforced (3D) C/Cs have been shown to possess remarkably low shear strength and yet high strain capability [5]. For example, a tensile strength of 250 MPa and a shear strength of 20 MPa was reported for an orthogonal 3D-C/C [5]. As a result, these poor properties are often critical parameters in the context of designing C/C structures.

The evaluation of shear behavior at elevated temperatures remains a difficult task. Thermal expansion mismatch between a specimen and test fixtures prevents the utilization of test fixtures often employed for room-temperature shear tests, e.g., the Iosipescu shear-test configuration [59]. Aoki et al. [22] used an off-axis compressive tests method in which fibers were oriented at $\pm 45°$ to the loading direction. This method enabled the use of self-standing specimens, and thus the use of a supporting fixture at elevated temperatures can be avoided. Aoki et al. used dog bone specimens possessing a cross-section of 10 mm × 10 mm in the gauge section, as shown in Fig. 11. The shear stress τ and the shear strain γ were calculated according to the following equations [60]:

$$\tau = 0.5 \times P/A, \qquad \gamma = 2 \times \varepsilon_L, \tag{3}$$

where P, A, and ε_L denote the applied load, the cross-sectional area of the gauge section, and the strain in the longitudinal direction of specimen, respectively. The problem associated with this test method is that not only pure shear stress but also normal stress are applied to the fracture surface. Accordingly fracture shear stress might be affected by the normal stress.

Fig. 12 shows shear stress–strain (τ–γ) curves of an orthogonal 3D-C/C recorded at room temperature and also at elevated temperatures using the off-axis compressive method. The shear behavior represented by the τ–γ curves was divided roughly into three regions: (i) initial elastic, (ii) progressive non-linear, and (iii) nearly plateau stress regions. The initial shear modulus obtained in region (i) was as low as 2 GPa and loading capability did not degrade even at $\gamma > 10\%$. The onset stress of non-linearity and maximum shear stress regions significantly increased with an increase in the test temperature. To investigate the underlying mechanisms yielding substantial shear deformation and strength improvement at elevated temperatures, the evolution of shear damage was observed at different loading stages. At the transition strain from region (i) to region (ii), debonding at fiber bundle surfaces started to propagate; this lead to non-linearity in the τ–γ curve. In region (ii), the debonding of fiber bundles occurred progressively. When the debonding was completed, a nearly constant shear stress continued to be observed (region (iii)). In region (iii), the 3D-C/C was deformed by the sliding at fiber bundle interfaces. Fig. 11 shows the shear damage observed in a specimen deformed up to region (iii) at room temperature. This photograph clearly demonstrates that the shear damage spreads almost all over the fiber bundle interfaces. This finding indicates that the shear strength enhancement at elevated temperatures is attributed to the increase in the interfacial sliding stress of fiber bundles.

4.2. Shear fracture model

Based on above results, an analytical model was proposed by Aoki et al. for simulating the shear damage

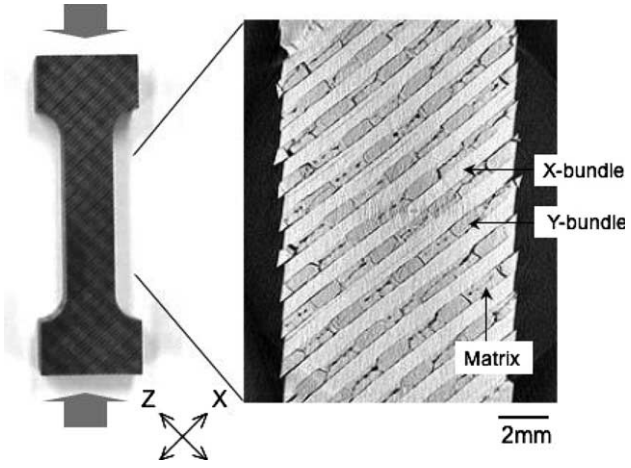

Fig. 11. Specimen geometry of the off-axis compressive test, and typical shear damage observed in the 3D-C/Cs after a shear strain γ of 10% [22].

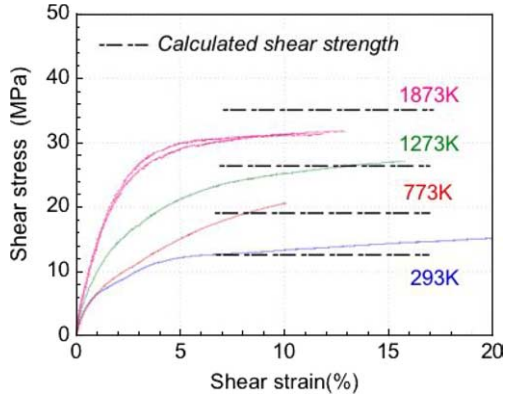

Fig. 12. Shear stress–strain curves of the orthogonal 3D-C/C at temperatures ranging from room temperature to 1873 K [22]. The dashed line represents predicted shear strength using Eq. (3).

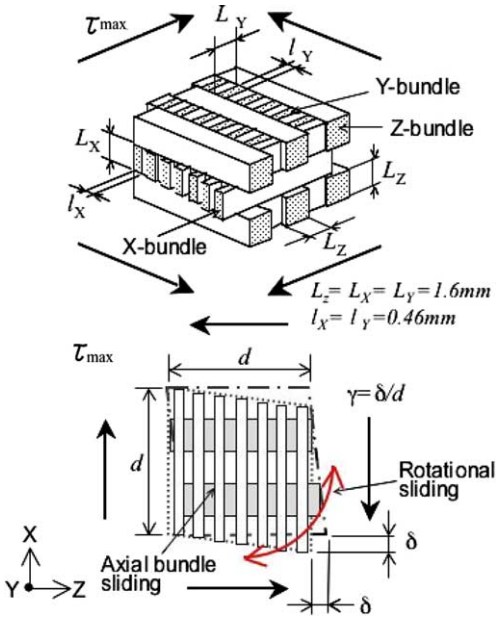

Fig. 13. Schematic drawing of shear deformation mechanisms observed in the 3D-C/C in the plateau shear-stress region [22].

process of a 3D-C/C [22]. This model was derived as a modification of Keith's model, which was originally developed for laminated composites [61]. In the present model, the shear damage of the 3D-C/C was simplified, as shown in Fig. 13. The applied load in the plateau stress region is sustained by two frictional sliding stresses, acting in the directions parallel and perpendicular to (rotational) fiber bundles. The sliding stresses τ_ss were determined by the fiber bundle push-out tests. Thus, the shear strength τ_{max} of the 3D-C/C can be expressed as [22]:

$$\tau_{max} = \frac{\pi}{2}\tau_s + 4\sum\left[\frac{\pi}{2}\frac{\tau_s}{L_z d^2}\int\int r^2\,\mathrm{d}r\,\mathrm{d}\phi\right], \tag{4}$$

where L_z and d denote the width of the z-bundles and the size of unit cell used for the calculations, respectively. The first and second terms represent the respective influences of axial bundle sliding and rotational sliding. Eq. (4) predicts high shear strength for composites with strong interfaces. The calculated τ_{max}s of the 3D-C/C are also indicated in Fig. 12 by the dashed lines. As can be seen in Fig. 12, reasonable agreement was observed between the calculated and the experimental shear strengths.

5. Compressive strength

The difficulty of evaluating the compressive strength of continuous fiber-reinforced composites is well known [62,63]. Compressive tests of composite materials have generally been carried out using a supporting jig in order to prevent premature bending deformation. Because C/Cs have extremely low shear modulus and strength [5,64], prevention of such bending deformation during compression tests is of primary concern. However, the supporting jig approach is difficult to apply at elevated temperatures, due to the difficulty of avoiding a thermal expansion mismatch between the specimen and the test fixtures.

The compressive fracture mechanisms of fiber-reinforced composites are classified into three categories, i.e., compressive failure of the fiber, shear failure, and kinking [62,63,65]. Among these, kinking is the most frequently observed. This type of fracture tends to be preceded by the micro-buckling of the fiber. The micro-buckling stress σ_c has been discussed by a number of groups [66–68]; the following (or a similar) criterion has been given for the onset of fiber buckling;

$$\sigma_c = \frac{G_m}{1 - V_f}, \tag{5}$$

where G_m is the shear modulus of the matrix and V_f is a volume fraction of load supporting fibers. This equation is known to be quantitatively incorrect, but has been nonetheless employed to predict qualitative tendencies [68,69].

As regards the compressive fracture behavior of C/Cs, little data are available. In particular, very little is known about high-temperature results. Fitzer [70] and Monacha [71] first examined the compressive strength of C/Cs, and more recently Gupta et al. [72–75] and Kishi et al. [76,77] have reported more detailed results obtained at room temperature. Gupta et al. examined the compressive fracture behavior of laminated C/C reinforced with eight harness satin weave cloths using rectangular parallelepiped block specimens. They concluded that the compressive failure of the C/C finally results in interlaminar shear fracture, but the initial failure is a kink originating from an internal defect such as interfacial debonding between the fiber and the matrix. Kishi et al. also observed similar results in an initial report [76], but when an inclined load against the fiber direction was applied in a unidirectionally reinforced C/C, they observed that in-plane shear fracture was dominated [77]. This result was apparently caused by the low shear strength of the C/Cs as noted above.

Hatta et al. [78] also investigated the compressive strength of a laminated and 3D-reinforced [10] C/Cs. As regards the laminated C/C, they observed interlaminar fracture under a compressive load, but the kink type of fracture was observed in the case of the 3D-C/C. Moreover, they examined the compressive strength of 3D-C/C at elevated temperatures up to 3000 K. The 3D-C/C had the tendency to induce kinks at the ends of the specimen, due to stress concentrations and its extremely low shear strength. In order to avoid this type of premature fracture and to conduct high-temperature

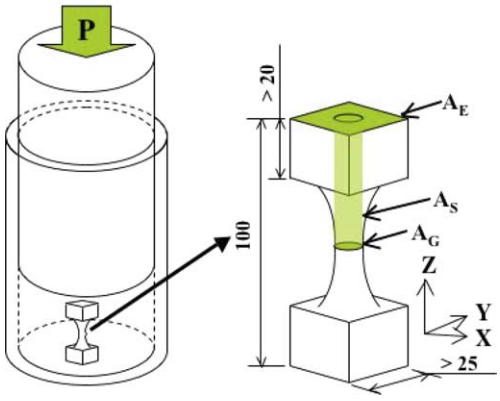

Fig. 14. The configuration of the compressive test, adopted for high-temperature tests of 3D-C/C, in which $A_E/A_G > 10$ and $A_S/A_G > 20$ in order to reduce stress concentration at the specimen ends and shear deformation effect [10].

tests, the specimen geometry and testing procedure were considered in detail. The configuration illustrated in Fig. 14 was found to be effective. This self-standing specimen was adopted in order to avoid thermal mismatch strain between the specimen and the test fixture at elevated temperatures; a sufficient loading area, A_E, and a shear supporting area, A_S, were arranged in order to alleviate the stress concentrations at specimen ends and to avoid shear deformation, respectively. Fig. 15 summarizes the results of high-temperature tensile and compressive tests of the 3D-C/C heat-treated at about 2800 K. As this figure depicts, the compressive strength of the 3D-C/C increased up to a temperature of 2273 K and decreased at temperatures beyond 2273 K.

The experimentally observed kinks (i.e., fiber fracture by bending) for the 3D-C/C were found to be the result of micro-buckling. Thus, Eq. (5) can be used to account for the compressive fracture. In the present cases, V_f in Eq. (5) should include only those fiber bundles oriented in the loading direction, and G_m should be taken as the shear modulus of the composite, including the matrix and fiber bundles oriented in directions other than in the loading direction. In Eq. (5), only G_m depends on temperature, and rough tendency of G_m can be obtained from Fig. 12. As shown in Fig. 12, G_m monotonically increased up to temperature of about 2000 K. Thus, the improvement in σ_c with an increase in temperature up to 2300 K can be explained in terms of G_m. Generally, the elastic modulus of the carbon material degrades at temperature higher than 2000 K [4]. This degradation explains the temperature dependence of σ_c in the region from 2000 to 2800 K. The rapid decreases in the compressive strength at temperatures exceeding 2800 K might be due to the degradation of the T300 fibers [9]. It should be noted here that 2800 K was heat treatment temperature of the 3D-C/C.

6. Fatigue behavior

Fatigue behavior is one of the most important design properties for primary load bearing structures intended for long-term use. However, only a few studies on the fatigue behavior of C/Cs have been reported [6,79–85]. Within authors' knowledge, fatigue data of C/Cs are available only at room temperature.

6.1. Fatigue in tension

6.1.1. S–N curves

The fracture strain vs. the number of cycles to failure, i.e., the *S–N* curves of unidirectionally reinforced (UD), cross-ply laminated (CP), and quasi-isotropically laminated (QI) C/Cs fatigue-tested at a frequency of 10 Hz, are shown in Fig. 16 [83]. The ultimate tensile failure strains obtained by static tensile tests were plotted as the data at a single fatigue cycle, $N = 1$. From Fig. 16, it is clear that the *S–N* curves of all of the C/Cs tested here were similar. The fracture strains gradually diminished from the static fracture strains to

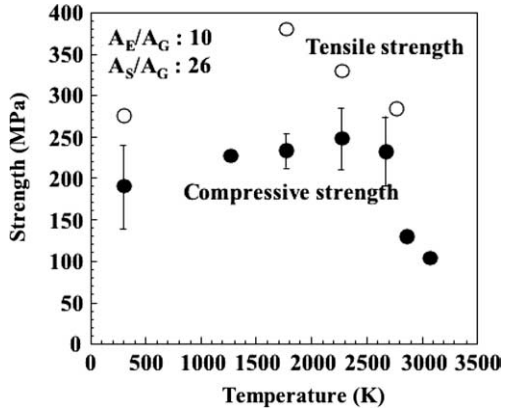

Fig. 15. Temperature dependence of compressive and tensile strengths of 3D-C/C [10].

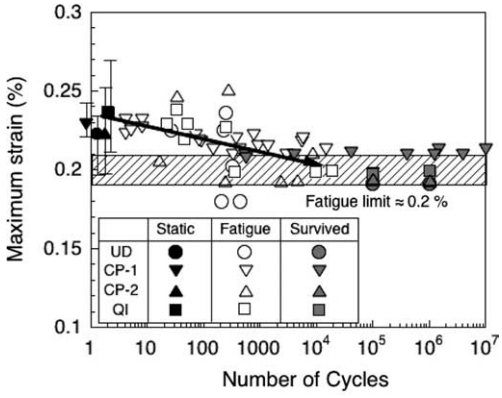

Fig. 16. Relationship between maximum strain and cycles to failure of 2D C/Cs subjected to fatigue loading [83].

fatigue limit strains of approximately $0.2 \pm 0.01\%$, and those limit strains were 85–92% of the static fracture strains. The fatigue limit cycle was ca. 10^4 cycles, and no fatigue fracture was observed beyond this cycle. This finding implies that the fatigue limits of the C/Cs were not affected by the fracture strain or fatigue limit of the matrix as is the case with carbon fiber-reinforced plastics, CFRPs [84].

6.1.2. Residual strength

The residual tensile fracture strains of the fatigue-loaded but surviving specimens were larger than the fatigue limit strains (≈0.2%), as shown in Figs. 17 (a) and (b). This finding accounts for the observation that no fatigue fractures were observed at over 10^4 cycles. This enhancement of the tensile strength was facilitated by increases in the number of fatigue cycles. In contrast, the C/Cs show slight increase in fracture strain with an increase in the maximum applied fatigue loading strain.

In order to characterize the micro-fractures that occurred during the fatigue loading in the principal load-bearing (0°) plies, a comparison of samples with and without clear strength enhancement caused by fatigue loading was carried out; the number of interfacial fractures and matrix cracks was compared between the samples [6]. Observation of cross-sections by SEM indicated

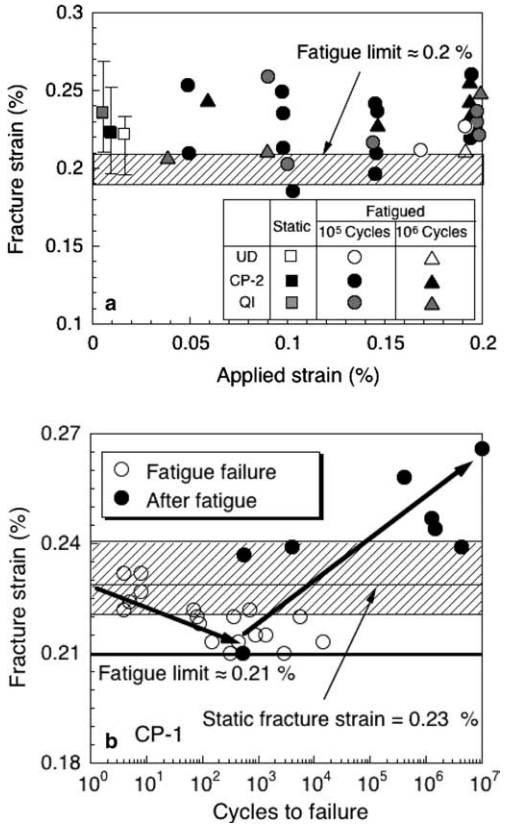

Fig. 17. Residual fracture strains after fatigue loading as functions of applied maximum fatigue strain (a) and applied cycles (b) [83].

that the strength enhancement mechanism required to recover or strengthen the C/Cs after fatigue was closely related to increases in the number of cracks near the fiber/matrix interfaces, i.e., the degradation of the fiber/matrix interface in 0° plies.

The *S–N* curves and residual failure strain after fatigue loading indicated that two types of damage occur during cyclic loading, namely degradation and enhancement of fracture strains of the 0° plies of the C/Cs. The first type of damage, i.e., the strength degradation mechanism, operated above the fatigue limit strain, and was most likely caused by fiber damage induced by wear due to sliding at interfaces, which is similar to the process that occurs in CFCCs [86–90]. The mechanism responsible for the other type of damage, i.e., enhancement of fracture strains, appeared to be the evolution of the fiber/matrix interface debonding, which had accumulated in the C/Cs during fatigue loading. As mentioned in Section 3.1, C/Cs have been reported to be strengthened by weakened fiber/matrix interface bonding [9,31,91].

6.2. Fatigue in shear mode

Absorbed water was found to reduce the static strength of C/Cs [8,49] and tensile fatigue behavior was also shown to be affected by absorbed water [85]. Shear mode fatigue tests were conducted in air, oil, or water using double-notched compression (DNC) specimens by Tanabe et al. [85]. They demonstrated that shear strength was reduced with fatigue loading under all conditions tested and water accelerated this degradation of strength. Strength degradation was slightly slower in oil than in air. These results suggest that fatigue degradation under shear loading occurred due to a wedge effect similar to the mechanism in CFCCs, and this effect was accelerated by stress corrosion cracking with water.

7. Concluding remarks

C/Cs exhibit high elastic modulus and brittle fracture under tensile loading, but low modulus and large fracture strain under shear loading. Although brittle fracture was observed under precisely controlled compressive loading, a slight inclination in compressive loading lead to large shear deformation. The present review showed that these characteristics are especially notable in 3D-C/Cs and are primarily derived from low interfacial strength (τ_d). The notch sensitivity of C/Cs, though not included in this review, is an important property for designing load-bearing structures. C/Cs are known to possess substantial toughness and notch insensitivity [5,91–93]. In particular, high toughness has been observed in 3D-C/Cs. Such high tough-

ness behavior was principally the result of extremely low τ_d values [5]. The combination of these characteristics is unique to C/Cs and is not congruous with existing design methodology. Thus, new design criteria are required to establish so as to effectively use C/Cs.

The low τ_d of C/Cs also affects other phenomena. For example, the low coefficient of the thermal expansion of C/Cs was partly caused by debonded fiber interfaces [27]. The fiber/matrix interface is thus an important research issue for understanding of various properties. However, investigations of the C/C interfaces remain at a primitive stage. For example, the interfacial shear strength shown in Figs. 2, 3, and 6 significantly varied when the test geometry changed [94]. Hence, research effort should be more actively directed to explore parameters that truly characterize interfacial fractures of C/Cs and their test methods.

References

[1] Buckley JD. Carbon–carbon materials and composite. NASA Ref Pub 1992;1254:267–81.

[2] Schmidt DL, Davidson KE, Theibert LS. Unique applications of carbon–carbon composites. SAMPE J 1999;35(3):27–39. 35(4):51–63; 35(5):47–55.

[3] Savage G. Carbon–carbon composites. Chapman & Hall; 1993.

[4] Thomas CR. Essentials of carbon–carbon composites. Royal Society of Chemistry; 1993.

[5] Aly-Hassan MS, Hatta H, Wakayama S, Watanabe M, Miyagawa K. Comparison of 2D and 3D carbon/carbon composites with respect to damage and fracture resistance. Carbon 2003;41:1069–78.

[6] Goto K, Hatta H, Katsu D, Machida T. Tensile fatigue of a laminated carbon–carbon composite at room temperature. Carbon 2003;41:1249–55.

[7] Kogo Y, Sumiya R, Hatta H, Sawada Y. Examination of strength-controlling factors in C/C composites using bundle composites. Adv Compos Mater 2003;12(2–3):139–54.

[8] Goto K, Hatta H, Oe M, Koizumi T. Tensile strength and deformation of a 2D carbon–carbon composite at elevated temperatures. J Am Ceram Soc 2003;86(12):2129–35.

[9] Hatta H, Aoi T, Kawahara I, Kogo Y, Shiota I. Tensile strength of carbon/carbon composites. J Compos Mater 2004;38(19):1667–89. 38(19):1685–99.

[10] Hatta H, Taniguchi K, Kogo Y. Compressive strength of three-dimensionally reinforced carbon/carbon composite. Carbon 2005;43:351–8.

[11] Marshall DB, Oliver WC. Measurement of interfacial mechanical properties in fiber-reinforced ceramic composites. J Am Ceram Soc 1987;70(8):542–8.

[12] Bianchi V, Goursat P, Sinkler W, Monthioux M, Menessier E. Carbon fiber-reinforced (YMAS) glass–ceramic matrix composites. III. Interfacial aspects. J Eur Ceram Soc 1984;19:317–27.

[13] Marshall DB, Oliver WC. An indentation method for measuring residual stresses in fiber-reinforced ceramics. Mater Sci Eng 1990;A126:95–103.

[14] Shetty DK. Shear-lag analysis of fiber push-out (indentation) tests for estimating interfacial friction stress in ceramic–matrix composites. J Am Ceram Soc 1988;71(2):C107–9.

[15] Honda K, Kagawa Y. Debonding criterion in the pushout process of fiber-reinforced ceramics. Acta Mater 1996;44(8): 3267–77.

[16] Kallas MN, Koss DA, Hahn HT, Hellmann JR. Interfacial stress state present in a "thin-slice" fiber push-out test. J Mater Sci 1992;27:3821–6.

[17] Zhou X-F, Wagner HD, Nutt SR. Interfacial propertied of polymer composites measured by push-out and fragmentation tests. Composites A 2001;32:1543–51.

[18] Serizawa H. The study about the physical properties of fiber-reinforced ceramics composites. PhD thesis, Tokyo University; 1997 [in Japanese].

[19] Fujita K, Sakai H, Iwashita N, Sawada Y. Influence of heat treatment temperature on interfacial shear strength of C/C. Proceedings of the 5th JPN international SAMPE symposium Tokyo 1997:1557–62.

[20] Sakai M, Matsuyama R, Miyajima T. The pull-out and failure of a fiber bundle in a carbon fiber reinforced carbon matrix composite. Carbon 2000;38:2123–31.

[21] Furukawa Y, Hatta H, Kogo Y. Interfacial shear strength of C/C composites. Carbon 2003;41:1819–26.

[22] Aoki T, Ogasawara T, Ishikawa T. Shear behavior and fiber bundle interfacial properties of 3D-C/C composites. Proceedings of the 8th international SAMPE JPN Tokyo 2003:845–8.

[23] Hatta H, Goto K, Ikegaki S, Kawahara I, Mohamed SAH, Hamada H. Tensile and fiber/matrix interfacial properties of 2D- and 3D-carbon/carbon composites. J Eur Ceram Soc 2005;25(4):535–42.

[24] Kawahara I, Hatta H, Siota I. Effects of interfacial strength on tensile fracture mechanism of C/C composites. Proceedings of the 8th Jpn international SAMPE symposium Tokyo 2003:18–21.

[25] Hatta H, Kawahara I, Goto Y, Siota I. Tensile strength of carbon/carbon composites III: effect of heat treatment temperature (pitch-based carbon fiber reinforced C/Cs). Carbon [submitted].

[26] Hatta H, Higuchi K, Kogo Y. Mechanisms of tensile fracture of C/C composites. Carbon [submitted].

[27] Hatta H, Kogo Y, Yoshihara Y, Sawada Y, Takahashi K, Hoshono K, et al. Thermal expansion behavior of C/C composites. Mater Syst 1995;14:15–24.

[28] Chang WC, Ma CCM, Tai NH, Chen CB. Effects of processing methods and parameters on the mechanical properties and microstructure of carbon/carbon composites. J Mater Sci 1994;29:5859–67.

[29] Domnanovich A, Peterlik H, Wanner A, Kromp K. Elastic moduli and interlaminar shear strength of a bidirectional carbon/carbon composite after heat treatment. Compos Sci Tech 1995;53:7–12.

[30] Manocha LM. The effect of heat treatment temperature on the properties of polyfurfuryl alcohol based carbon/carbon composite. Carbon 1994;32:213–23.

[31] Trouvat B, Bourrat X, Naslain R. Toughening mechanisms in C/C Minicomposites with Interface Control Ext Abst, 23rd Bi Conference Carbon. (Strasbourg): Am Carbon Soc 1997:536–7.

[32] Weisshaus H, Kenig S, Siegmann A. Effect of materials and processing on the mechanical properties of C/C composites. Carbon 1991;29:1203–20.

[33] Weisshaus H, Kening S, Kastner E, Siegmann A. Morphology development during processing of carbon–carbon composites. Carbon 1990;28:125–35.

[34] Rellick G. Densification efficiency of carbon–carbon composites. Carbon 1990;28(4):589–94.

[35] Hatta H, Suzuki K, Shigei T, Somiya S, Sawada Y. Strength improvement by densification of C/C composites. Carbon 2001;39:83–90.

[36] Aveston J, Cooper GA, Kelly A. Paper 2 Single and multiple fracture. Proc NPL 1973:15–26.

[37] Evans AG, Zok FW. The physics and mechanics of fiber-reinforced brittle matrix composites (Review). J Mater Sci 1994;29:3857–96.

[38] Curtin WA, Takeda N. Tensile strength of fiber-reinforced composites. J Compos Mater 1998;32(22):2042–59. 32(22):2060-81, 2000;34(15):1301-32.
[39] Curtin WA. Theory of mechanical properties of ceramic–matrix composites. J Am Ceram Soc 1991;74(11):2837–45.
[40] Evans AG, Domergue JM, Vagaggini E. Methodology for relating the tensile constituent properties. J Am Ceram Soc 1994;77(6):1425–35.
[41] Aveston J, Kelly A. Theory of multiple fracture of fibrous composites. J Mater Sci 1973;8:352–62.
[42] Fitzer E, Manocha LM. Carbon reinforcements and carbon/carbon composites. Sparinger 1998(Chap6):190–236.
[43] Kendall K. Transition between cohesive and interfacial failure in a laminate. Proc Roy Soc Lond SerA 1975;344:287–302.
[44] Hatta H, Nakayama Y, Kogo Y. Bonding strength of SiC coating on the surface of C/C composite. Adv Compos Mater 2004;13(2):141–56.
[45] Rebillat F, Lamon J, Guette A. The concept of a strong interface applied to SiC/SiC composites with a BN interphase. Acta Mater 2000;48:4609.
[46] Kogo Y, Kikkawa A, Saito W, Hatta H. Comparative study on tensile fracture behavior of monofilament and bundle C/C composites. In: Proceedings of the 11th US-JPN conference composite material 2004-9, Yonezawa JPN; C/C1.1–1.4.
[47] Hatta H, Kogo Y, Okura A. Research report for new energy and industrial technology development organization, NEDO-ITK-9209; 1993 [in Japanese].
[48] Sato S, Kurumada A, Iwaki H, Komatsu Y. Tensile properties and fracture toughness of carbon-fiber felt reinforced carbon composites at high temperature. Carbon 1989;27:791–801.
[49] Kogo Y, Hatta H, Okura A, Fujikura M, Seimiya Y. Bending and interlaminar properties of C/C composite at elevated temperatures. Tanso (Carbon) 1995;166:40–6 (in Japanese).
[50] Rowe GW. High temperature strength of clean graphite. Nucl Eng March 1962:102–3.
[51] Maruyama T, Nishimura Y. Effect of absorbed gases on mechanical properties of nuclear graphite. Tanso (Carbon) 1992;152:98–105 (in Japanese).
[52] Koyama M, Hatta H, Fukuda H, Bando T. Strength of carbon bonding between C/C composites at elevated temperatures. Carbon 2004;43:171–7.
[53] Sines G, Yang Z, Vickers BD. Creep of carbon yarn and a carbon–carbon composite at high temperature and high stress. Carbon 1989;27(3):403–15.
[54] Fujikura M. Ultra-high temperature materials research center Co. Ltd., Japan. unpublished work.
[55] Dorn JE. Some fundamental experiments on high temperature creep. Creep and fracture of metals at high temperature. National Physical Laboratory Symposium 1954. London: HMSO; 1956. p. 89–138.
[56] Hawthone HM. The mechanics of stretch-graphitization of glassy carbon fibers. J Mater Sci 1976;11:97–110.
[57] Goto K, Hatta H, Takahashi H, Kawada H. Effects of shear damage on the fracture behavior of carbon–carbon composites. J Am Ceram Soc 2001;84(6):1327–33.
[58] Denk L, Hatta H, Misawa A, Somiya S. Shear fracture of C/C composites with variable stacking sequence. Carbon 2001;39:1505–13.
[59] Iosipescu N. New accurate procedure for single shear testing of metals. Rev Mec Appl 1963;1:145–64.
[60] Ho H, Tsai MY, Morton J. A comparison of three popular test methods for determining the shear modulus of composite materials. Compos Eng 1993;3(1):69–81.
[61] Keith WP, Kedward KT. Shear damage mechanisms in a woven, Nicalon-reinforced ceramic–matrix composite. J Am Ceram Soc 1997;80(2):357–64.
[62] Hull D. An introduction to composite materials. Cambridge: Cambridge Univ. Press; 1981. p. 154–63.
[63] Jones RM. Mechanics of composite materials. Tokyo: McGrow-Hill Kogakusha; 1975. p. 134–43.
[64] Evans AG, Zok FW. Review: The physics and mechanics of fiber-reinforced brittle matrix composites. J Mater Sci 1994(29):3857–96.
[65] Piggot MR. A theoretical framework for the compressive properties of aligned fiber composites. J Mater Sci 1981;15:2523–38.
[66] Rosen WB, Dow NF, Hashin Z. Mechanical properties fibrous composites. NASA CR-31 April, 1964. 66. Dow NF, Rosen WB. Evaluation of filament-reinforced composites for aerospace structural applications. NASA CR-207 April, 1965.
[67] Dow NF, Rose WB. Evaluation of filament-reinforced composites for aerospace structural applications. NASA CR-207 April, 1965.
[68] Hahn HT, Soni M, Moon S. Compression failure mechanisms of composite structures NASA CR-3988 June, 1986.
[69] Steif PS. Simple model for the compressive failure of weakly bonded fiber-reinforced composites. J Compos Mater 1988;22:818–28.
[70] Fitzer F. The future of carbon–carbon composites. Carbon 1987;25:163.
[71] Manocha LM, Bahl OP. Influence of carbon fiber type and weave pattern on the development of 2D carbon–carbon composites. Carbon 1988;26:13.
[72] Gupta V, Anand K, Kryska M. Failure mechanisms of laminated carbon–carbon composites-I. Under uniaxial compression. Acta Meta 1994;42(3):781–95.
[73] Grape JA, Gupta V. Failure mechanisms in laminated carbon–carbon composites under biaxial compression. Acta Mater 1995;43(7):2657–65.
[74] Anand K, Gupta V. The effect of processing conditions on the compressive and shear strength of 2D carbon–carbon laminates. Carbon 1995;33(6):739–48.
[75] Anand K, Gupta V, He Y-M. A numerical study of the compression and shear failure of woven carbon–carbon laminates. J Compos Mater 1995;29(18):2446–63.
[76] Tohyama N, Kim BN, Enoki M, Kishi T. Compressive strength and failure mechanisms of laminated C/C composites by using acoustic emission method. Mater Trans JIM 1996;37(5):1156–60.
[77] Kim BN, Tohyama N, Enoki M, Kishi T. Shear and compressive strengths of uni-directionally reinforced C/C composit. Trans JSME (A) 1997;63(614):2149–54.
[78] Kogo Y, Hatta H, Misawa A. Compressive behavior of carbon–carbon composites. In: Proceedings of the 4th Japan international SAMPE symposium; 1995. p. 1159–64.
[79] Hatta H, Kogo Y, Tanimoto T, Morii T. Static and fatigue fracture behavior of C/C composites. In: Proceedings of the 4th Japan international SAMPE symposium; 1995. p. 368–73.
[80] Rouby D, Reynaud P. Fatigue behavior related to interface modification during load cycling in ceramic–matrix fibre composites. Comp Sci Technol 1993;48:109–18.
[81] Tallaron C, Rouby D, Reynaud P, Fantozzi G. Improvement of cyclic fatigue analysis by the use of a tensile master curve in carbon/carbon composites. Key Eng Mater 1999;164–165:329–32.
[82] Ozturk A, Moore RE. Tensile fatigue behavior of tightly woven carbon/carbon composites. Composites 1992;23:39–46.
[83] Goto K, Furukawa Y, Hatta H, Kogo Y. Fatigue behavior of 2D laminate C/C composites at room temperature. Comp Sci Technol 2005;65(7–8):1044–51.
[84] Talreja R. Structure and properties of composites. In: Chou TW, editor. Fatigue of fiber composites. Tokyo: VCW; 1993. p. 583–608 [chapter 13].
[85] Tanabe Y, Yoshimura T, Watanabe T, Hiraoka T, Ogita Y, Yasuda E. Fatigue of C/C composites in bending and in shear modes. Carbon 2004;42:1665–70.
[86] Sorensen BF, Holmes JW, Vanswijgenhoven EL. Rate of strength decrease of fiber-reinforced ceramic-matrix composites during fatigue. J Am Ceram Soc 2000;83(6):1469–75.

[87] Shuler SF, Holmes JW, Wu X, Roach D. Influence of loading frequency on the room-temperature fatigue of a carbon-fibers/SiC-matrix composite. J Am Ceram Soc 1993;76(9):2327–36.
[88] Chawla N, Tur YK, Holmes JW, Barber JR, Szweda A. High-frequency fatigue behavior of woven-fiber-fabric-reinforced polymer-derived ceramic–matrix composites. J Am Ceram Soc 1998;8(5):1221–30.
[89] Staehler JM, Mall S, Zawada LP. Frequency dependence of high-cycle fatigue behavior of CVI C/SiC at room temperature. Comp Sci Technol 2003;63:2121–31.
[90] Mizuno M, Zhu S, Nagano Y, Sakaida Y, Kagawa Y, Watanabe M. Cyclic-fatigue behavior of SiC/SiC composites at room and high temperatures. J Am Ceram Soc 1996;79(12):3065–77.
[91] Kogo Y, Hatta H, Kawada H, Machida T. Effect of stress concentration on tensile fracture behavior of carbon–carbon composites. J Comp Mater 1998;32(13):1273–94.
[92] Denk L, Hatta H, Somiya S, Misawa H. Fracture behaviour of multi-holed C/C composites. Adv Compos Mater 2003;12(2–3):107–22.
[93] Aly-Hassan MS, Hatta H, Wakayama S. Effect of zigzag damage extension mechanism on fracture toughness of cross-ply laminated carbon/carbon composites. Adv Compos Mater 2003;12(2–3):223–36.
[94] Goto K, Kawahara I, Hatta H, Kogo Y, ShiotaI. Measurement of fiber/matrix interface properties of C/C composites by single fiber and fiber bundle push-out methods. Compos Interf [accepted].